

## Article

# Effects of Coarse Aggregate Maximum Size on Synthetic/Steel Fiber Reinforced Concrete Performance with Different Fiber Parameters

Haider M. Al-Baghdadi <sup>1</sup>, Faiz H. Al-Merib <sup>1</sup>, Ayooob A. Ibrahim <sup>1</sup>, Rafea F. Hassan <sup>1</sup> and Husam H. Hussein <sup>2,\*</sup> 

<sup>1</sup> Department of Civil Engineering, College of Engineering, University of Babylon, Babylon, Iraq; eng.haider.m@uobabylon.edu.iq (H.M.A.-B.); eng.faiz.hussein@uobabylon.edu.iq (F.H.A.-M.); eng.ayooob.ibrahim.lec@uobabylon.edu.iq (A.A.I.); eng.rafea.flaih@uobabylon.edu.iq (R.F.H.)

<sup>2</sup> Department of Civil Engineering, Ohio University, Athens, OH 45701, USA

\* Correspondence: hh236310@ohio.edu

**Abstract:** Recently, fiber has been incorporated into concrete mixtures, where its distribution in the concrete matrix helps to improve and enhance the mechanical properties of fiber-reinforced concrete (FRC). The aim of this study is to investigate the influence of steel and synthetic fiber parameters, along with different coarse aggregate maximum sizes (CAMZs) on FRC performance. Additionally, in past research, the empirical relationships among the compressive, tensile, and flexural strengths of plain concrete and FRC were assessed, and correlations between these mechanical properties of FRC were examined. For each CAMZ, four fiber dosages for each fiber type were considered. The results demonstrate the mechanical properties of FRC enhanced as the fiber length increased from 13 mm to 60 mm, the CAMZ increased from 9.5 mm to 37.5 mm, and the ratio of the fiber length to the CAMZ was in the range of 0.35–5.68. All mixtures have been intended to exhibit similar compressive strengths; however, the synthetic/steel fiber advanced the brittleness ratio of specimens with G10, G19, and G38 to approximately 36.8%, 40.7%, and 47.4% greater than the control specimens, respectively. In addition, from the regression analysis investigation, there are strong correlations from the regression analysis of the mechanical property results of FRC.

**Keywords:** coarse aggregate maximum size; synthetic fiber; steel fiber; fiber-reinforced concrete



**Citation:** Al-Baghdadi, H.M.; Al-Merib, F.H.; Ibrahim, A.A.; Hassan, R.F.; Hussein, H.H. Effects of Coarse Aggregate Maximum Size on Synthetic/Steel Fiber Reinforced Concrete Performance with Different Fiber Parameters. *Buildings* **2021**, *11*, 158. <https://doi.org/10.3390/buildings11040158>

Academic Editor: Pavel Reiterman

Received: 17 March 2021

Accepted: 6 April 2021

Published: 13 April 2021

**Publisher's Note:** MDPI stays neutral with regard to jurisdictional claims in published maps and institutional affiliations.



**Copyright:** © 2021 by the authors. Licensee MDPI, Basel, Switzerland. This article is an open access article distributed under the terms and conditions of the Creative Commons Attribution (CC BY) license (<https://creativecommons.org/licenses/by/4.0/>).

## 1. Introduction

Concrete is identified to be weak in resisting tensile stresses and can easily crack under low-level tensile forces. Incorporating fiber into the concrete mixture is a typical method to modify concrete material. Due to the distribution of fiber in the concrete mixture, the mechanical properties of fiber-reinforced concrete (FRC) might be improved. The amount of enhancement of the performance of a concrete structure is mainly proportional to the volume fraction, aspect ratio, fiber geometry, fiber distribution, and fiber orientation [1–8].

One of the effects on the fiber orientation and distribution in the concrete matrix is the coarse aggregate maximum size (CAMZ), which significantly impacts the mechanical properties of FRC. With the CAMZ increased from 3 mm to 14 mm, the tensile strength and elasticity modulus reduce, while the fracture energy of concrete specimens is enhanced [9]. Appa Rao and Raghu Prasad [10] found that the fracture toughness and fracture energy of concrete were enhanced due to the increase of the CAMZ from 4.75 mm to 20 mm.

Past research has investigated the effect of CAMZs of 8, 13, and 20 mm and fiber dosages of 0.0%, 1.0%, and 2.0% on the flexural performance of steel FRC [11–14]. According to Olivito and Zuccarelli [15], to ensure a uniform and efficient fiber distribution, the steel fiber length should be two times more than the CAMZ. Additionally, steel FRC with a small CAMZ shows better flexural behavior, and the CAMZ of steel FRC should not go beyond a three-quarter steel fiber length [16]. The ratio of the length of the steel fiber to the CAMZ influences the mechanical properties of steel FRC as much as the fiber content.

The steel fiber parameters have substantial effects on the properties of FRC. FRC with a 60 mm length of steel fiber exhibits higher flexural strength and fracture strength than the concrete with a 30 mm steel fiber length [17,18]. On the other hand, Doo-Yeol Yoo et al. [19,20] reported that the incorporation of a 30 mm fiber length in concrete showed less improvement in flexural performance compared with the FRC with a 13–19.5 mm fiber length. Other fiber parameters that impact the FRC properties are the fiber type and fiber shape, which may influence the dynamic and static concrete properties [21]. The distribution and orientation of steel fiber have considerably influenced concrete performance [22–25]. According to the investigations of Mert Yücel Yardimci et al. [26] and Lee and Kim [27], the CAMZ and properties of steel fiber influence the fiber fracture energy and orientation of steel FRC. In addition, another study by Su Tae Kang et al. [28] reported that the ultimate flexural strength of steel FRC was mainly affected by the fiber distribution characteristics, with less impact on the first cracking strength.

Research to date on using steel fiber in concrete mixtures indicates an improvement in the mechanical properties of FRC. However, there is no study examining the effect of the CAMZ on the behavior of synthetic FRC. Additionally, for steel FRC, past research has investigated the impact of CAMZs less than 25 mm on concrete performance, along with limited studies on CAMZs larger than 25 mm. Therefore, in order to find optimal fiber strengthening and toughening with different CAMZs, it is necessary to understand the correlations among the flexural, splitting tensile, and compressive strengths of synthetic/steel FRC with different fiber parameters. Studies about the relationship between fiber parameters and CAMZs of FRC are limited.

## 2. Objectives

The aim of this study is to investigate the impact of the steel and synthetic fiber parameters (fiber length, diameter, and shape), along with the CAMZ, on the workability, compressive, tensile, and flexural strengths of FRC. The fiber length ( $l_f$ ) from 13 mm to 60 mm, CAMZ from 9.5 mm to 37.5 mm, and ratio of  $l_f$ /CAMZ in the range of 0.35–5.68 were conducted in order for the results to be used in the proposed logical range of the  $l_f$ /CAMZ ratio. For each CAMZ, four fiber dosages of 0.0%, 0.5%, 1.0%, and 1.5% by the volume of concrete for each fiber type were considered. Moreover, in this research, correlations among the flexural, splitting tensile, and compressive strengths of synthetic/steel FRC with different fiber parameters were analyzed and evaluated with past research empirical relations.

## 3. Experimental Program

### 3.1. Materials

The composition of Portland cement (Type I) utilized in this study is listed in Table 1, in accordance with ASTM C150-04a [29]. In Table 2, the physical composition of the cement is presented along with the ASTM C150-04a [29] limits. River sand (fine aggregate) passed through a 4.75 mm sieve was used. The sieve analysis of the fine aggregate and the passing of the overall limit of ASTM C33-03 [30] are listed in Table 3. For the coarse aggregate, three CAMZs were used (CAMZ = 9.5 mm, 19 mm, and 37.5 mm), namely G10, G19, and G38, respectively. The sieve analysis of the coarse aggregates is listed in Table 4. This table shows that the grading of the coarse aggregate was within the ASTM C33-03 [30] limits.

Three fiber configurations, namely micro steel fiber, hooked end steel fiber, and macro synthetic fiber, were used. For the micro steel fiber (HAREX copper-plated micro-filament steel fiber), the fiber length was 13 mm. In addition, for the hooked end steel fiber (HAREX fiber), lengths of 35 mm and 60 mm were used. Fiber lengths of 19, 38, and 54 mm were used for the macro synthetic fiber (Forta Ferro concrete fiber). The properties of the studied fibers are listed in Table 5, and Figure 1 shows a photo of each fiber type.

**Table 1.** Portland cement composition.

Constituent	Chemical Composition	Cement (Type I) % by Weight **	ASTM C150-04a [29]
Aluminum oxide	Al <sub>2</sub> O <sub>3</sub>	5.45	—
Iron oxide	Fe <sub>2</sub> O <sub>3</sub>	3.41	—
Magnesia	MgO	3.7	6.0 *
Sulfate	SO <sub>3</sub>	2.25	3.0 *
Loss on ignition	L.O.I	1.68	3.0 *
Insoluble residue	I.R	0.42	0.75 *
Tricalcium aluminates	C <sub>3</sub> A	9.85	—
Tricalcium silicate	C <sub>3</sub> S	40.43	—
Dicalcium silicate	C <sub>2</sub> S	28.1	—
Tricalcium alumina ferrite	C <sub>4</sub> AF	8.12	—

\* Maximum limit. \*\* Tested by the authors.

**Table 2.** Physical composition of the cement.

Physical Properties	ASTM C150-04a [29]	Test Results ***
Finesses, specific surface (m <sup>2</sup> /kg)		
Turbidimeter test	160 **	190
Air permeability	280 **	310
Soundness using autoclave method	0.8% *	0.12%
Setting time at which Vicat's instrument was used		
Initial (min)	45 **	120
Final (min)	375 *	280
Compressive strength for the cement paste cube		
3 days (MPa)	12 **	16
7 days (MPa)	19 **	25

\* Maximum limit. \*\* Minimum limit. \*\*\* Tested by the authors.

**Table 3.** Sieve analysis of the fine aggregate.

Sieve Size (mm)	Cumulative Passing % *	% Passing of the Overall Limit of ASTM C33-03 [30]
9.5	100	100–100
4.75	97	95–100
2.36	92	80–100
1.18	72	50–85
0.6	41	25–60
0.3	14	5–30
0.15	4	0–10

\* Tested by the authors.

### 3.2. Mix Design

Several concrete mixes were conducted to investigate the effects of different fiber types, including fiber configurations, fiber materials, and CAMZs, on the mechanical properties of FRC. The mix proportions of the concrete series are listed in Table 6. The water-to-cement ( $w/c$ ) ratio was 0.45 for all mixes. For each CAMZ, four fiber dosages of 0.0%, 0.5%, 1.0%, and 1.5% by the volume of concrete for each fiber type were considered. A total of 57 FRC mixes, including three control mixes (0.0% fiber dosage), were prepared in this study, as shown in Table 7. The mixes were given identification numbers, as shown in Figure 2.

**Table 4.** Sieve analysis of the coarse aggregate.

Aggregate ID	Sieve Size (mm)	Cumulative Passing % *	% Passing of the Overall Limit of ASTM C33-03 [30]
G10	9.5	96	85–100
	4.75	25	10–30
	2.36	8	0–10
	1.18	0	0–5
G19	19	98	90–100
	9.5	51	20–55
	4.75	4	0–10
G38	37.5	96	95–100
	19	45	35–70
	9.5	21	10–30
	4.75	3	0–5

\* Tested by the authors.

**Table 5.** Properties of fibers provided by the manufacturer.

Fiber ID	Fiber Type	Material	Length (lf) (mm)	Diameter (df) (mm)	Aspect Ratio (lf/df)	Tensile Strength MPa
MSF-13	Micro steel fiber	Steel	13	0.2	65	>2100
HSF-35	Hooked end steel fiber	Steel	35	0.55	64	900–2200
HSF-60	Hooked end steel fiber	Steel	60	0.75	80	900–2200
SYF-19	Macro synthetic fiber	Copolymer/Polypropylene	19	0.34	56	570–660
SYF-38	Macro synthetic fiber	Copolymer/Polypropylene	38	0.34	112	570–660
SYF-54	Macro synthetic fiber	Copolymer/Polypropylene	54	0.34	168	570–660



(a)



(b)



(c)



(d)



(e)



(f)

**Figure 1.** (a) MSF-13, (b) HSF-35, (c) HSF-60, (d) SYF-19, (e) SYF-38, and (f) SYF-54 fibers.

Table 6. Mix constituents.

Constituents	Mix Number		
	Mix 1	Mix 2	Mix 3
Cement (Kg/m <sup>3</sup> )	450	450	450
Water (Kg/m <sup>3</sup> )	203	203	203
Water/cement ratio ( <i>w/c</i> )	0.45	0.45	0.45
Sand (Kg/m <sup>3</sup> )	723	723	723
Coarse aggregate (Kg/m <sup>3</sup> )	1010	1010	1010
CAMZ (mm)	9.5	19	37.5
Aggregate ID	G10	G19	G38
Fiber content (%) by volume	0/0.5/1.0/1.5	0/0.5/1.0/1.5	0/0.5/1.0/1.5

Table 7. Fiber-reinforced concrete (FRC) mixes.

Mix with CAMZ of 9.5 mm (G10)				Mix with CAMZ of 19 mm (G19)				Mix with CAMZ of 37.5 mm (G38)			
Mix ID	Fiber ID	Dosage	lf/CAMZ	Mix ID	Fiber ID	Dosage	lf/CAMZ	Mix ID	Fiber ID	Dosage	lf/CAMZ
Con-G10	–	0.0%	–	Con-G19	–	0.0%	–	Con-G38	–	0.0%	–
MSF-13-0.5-G10	MSF-13	0.5%	1.37	MSF-13-0.5-G19	MSF-13	0.5%	0.68	MSF-13-0.5-G38	MSF-13	0.5%	0.35
MSF-13-1.0-G10	MSF-13	1.0%	1.37	MSF-13-1.0-G19	MSF-13	1.0%	0.68	MSF-13-1.0-G38	MSF-13	1.0%	0.35
MSF-13-1.5-G10	MSF-13	1.5%	1.37	MSF-13-1.5-G19	MSF-13	1.5%	0.68	MSF-13-1.5-G38	MSF-13	1.5%	0.35
HSF-35-0.5-G10	HSF-35	0.5%	3.68	HSF-35-0.5-G19	HSF-35	0.5%	1.84	HSF-35-0.5-G38	HSF-35	0.5%	0.93
HSF-35-1.0-G10	HSF-35	1.0%	3.68	HSF-35-1.0-G19	HSF-35	1.0%	1.84	HSF-35-1.0-G38	HSF-35	1.0%	0.93
HSF-35-1.5-G10	HSF-35	1.5%	3.68	HSF-35-1.5-G19	HSF-35	1.5%	1.84	HSF-35-1.5-G38	HSF-35	1.5%	0.93
HSF-60-0.5-G10	HSF-60	0.5%	6.32	HSF-60-0.5-G19	HSF-60	0.5%	3.16	HSF-60-0.5-G38	HSF-60	0.5%	1.60
HSF-60-1.0-G10	HSF-60	1.0%	6.32	HSF-60-1.0-G19	HSF-60	1.0%	3.16	HSF-60-1.0-G38	HSF-60	1.0%	1.60
HSF-60-1.5-G10	HSF-60	1.5%	6.32	HSF-60-1.5-G19	HSF-60	1.5%	3.16	HSF-60-1.5-G38	HSF-60	1.5%	1.60
SYF-19-0.5-G10	SYF-19	0.5%	2.00	SYF-19-0.5-G19	SYF-19	0.5%	1.00	SYF-19-0.5-G38	SYF-19	0.5%	0.51
SYF-19-1.0-G10	SYF-19	1.0%	2.00	SYF-19-1.0-G19	SYF-19	1.0%	1.00	SYF-19-1.0-G38	SYF-19	1.0%	0.51
SYF-19-1.5-G10	SYF-19	1.5%	2.00	SYF-19-1.5-G19	SYF-19	1.5%	1.00	SYF-19-1.5-G38	SYF-19	1.5%	0.51
SYF-38-0.5-G10	SYF-38	0.5%	4.00	SYF-38-0.5-G19	SYF-38	0.5%	2.00	SYF-38-0.5-G38	SYF-38	0.5%	1.01
SYF-38-1.0-G10	SYF-38	1.0%	4.00	SYF-38-1.0-G19	SYF-38	1.0%	2.00	SYF-38-1.0-G38	SYF-38	1.0%	1.01
SYF-38-1.5-G10	SYF-38	1.5%	4.00	SYF-38-1.5-G19	SYF-38	1.5%	2.00	SYF-38-1.5-G38	SYF-38	1.5%	1.01
SYF-54-0.5-G10	SYF-54	0.5%	5.68	SYF-54-0.5-G19	SYF-54	0.5%	2.84	SYF-54-0.5-G38	SYF-54	0.5%	1.44
SYF-54-1.0-G10	SYF-54	1.0%	5.68	SYF-54-1.0-G19	SYF-54	1.0%	2.84	SYF-54-1.0-G38	SYF-54	1.0%	1.44
SYF-54-1.5-G10	SYF-54	1.5%	5.68	SYF-54-1.5-G19	SYF-54	1.5%	2.84	SYF-54-1.5-G38	SYF-54	1.5%	1.44

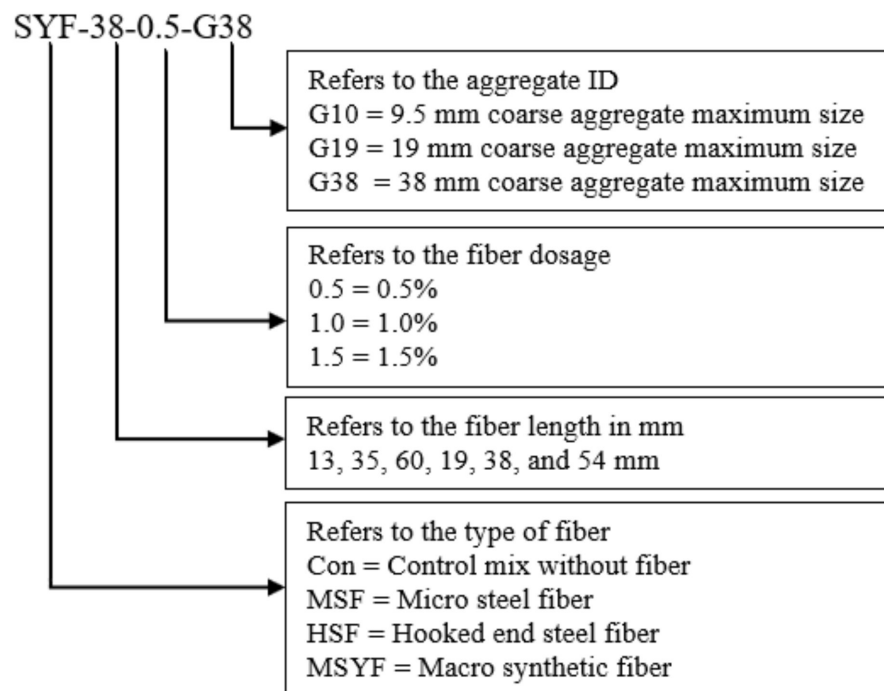


Figure 2. Mix identification chart.

### 3.3. Specimen Preparation

For specimen preparation, the constituents of the FRC mixes listed in Table 6 were prepared and cast in cubes, cylinders, and prisms for compressive strength [31], tensile strength [32], and flexural strength [33], respectively. After mixing all concrete constituents, the fiber was added to prevent fiber balls and to ensure the fiber was distributed uniformly through the mixes. A total of 3 cubes (150 mm × 150 mm × 150 mm), 3 cylinders (152 mm × 305 mm), and 3 prisms (100 mm × 100 mm × 500 mm) were cast in this study for each concrete design mixture, as depicted in Table 8. Therefore, the total number of specimens was 513 specimens. After one day, the specimens were separated from the molds. Then, the specimens were completely submerged in water for 28 days and removed from the water before the testing day, in accordance with ASTM C31/C31M [34].

Table 8. Brittleness ratio of synthetic/steel FRC.

Specimen ID	Brittleness Ratio	Diff. %	Specimen ID	Brittleness Ratio	Diff. %	Specimen ID	Brittleness Ratio	Diff. %
Con-G10	9.50	0.0%	Con-G19	9.14	0.0%	Con-G38	8.78	0.0%
MSF-13-0.5-G10	7.49	−21.2%	MSF-13-0.5-G19	7.67	−16.0%	MSF-13-0.5-G38	8.22	−6.4%
MSF-13-1.0-G10	7.67	−19.3%	MSF-13-1.0-G19	7.46	−18.3%	MSF-13-1.0-G38	7.29	−16.9%
MSF-13-1.5-G10	7.68	−19.2%	MSF-13-1.5-G19	7.67	−16.1%	MSF-13-1.5-G38	7.45	−15.1%
HSF-35-0.5-G10	10.71	12.7%	HSF-35-0.5-G19	8.83	−3.4%	HSF-35-0.5-G38	7.93	−9.6%
HSF-35-1.0-G10	7.90	−16.9%	HSF-35-1.0-G19	6.69	−26.8%	HSF-35-1.0-G38	5.95	−32.2%
HSF-35-1.5-G10	7.04	−26.0%	HSF-35-1.5-G19	5.70	−37.6%	HSF-35-1.5-G38	6.43	−26.7%
HSF-60-0.5-G10	9.96	4.8%	HSF-60-0.5-G19	8.46	−7.4%	HSF-60-0.5-G38	7.75	−11.7%
HSF-60-1.0-G10	8.66	−8.9%	HSF-60-1.0-G19	6.53	−28.5%	HSF-60-1.0-G38	5.44	−38.0%
HSF-60-1.5-G10	6.92	−27.2%	HSF-60-1.5-G19	5.81	−36.4%	HSF-60-1.5-G38	4.62	−47.4%

Table 8. Cont.

Specimen ID	Brittleness Ratio	Diff. %	Specimen ID	Brittleness Ratio	Diff. %	Specimen ID	Brittleness Ratio	Diff. %
SYF-19-0.5-G10	7.10	−25.3%	SYF-19-0.5-G19	7.24	−20.7%	SYF-19-0.5-G38	6.81	−22.4%
SYF-19-1.0-G10	6.60	−30.5%	SYF-19-1.0-G19	6.57	−28.1%	SYF-19-1.0-G38	6.25	−28.8%
SYF-19-1.5-G10	6.30	−33.8%	SYF-19-1.5-G19	6.56	−28.2%	SYF-19-1.5-G38	6.03	−31.3%
SYF-38-0.5-G10	6.90	−27.4%	SYF-38-0.5-G19	6.72	−26.4%	SYF-38-0.5-G38	6.12	−30.2%
SYF-38-1.0-G10	6.23	−34.4%	SYF-38-1.0-G19	5.97	−34.7%	SYF-38-1.0-G38	5.22	−40.5%
SYF-38-1.5-G10	6.10	−35.8%	SYF-38-1.5-G19	5.47	−40.1%	SYF-38-1.5-G38	5.05	−42.4%
SYF-54-0.5-G10	6.04	−36.4%	SYF-54-0.5-G19	6.53	−28.5%	SYF-54-0.5-G38	5.78	−34.1%
SYF-54-1.0-G10	6.16	−35.2%	SYF-54-1.0-G19	5.42	−40.7%	SYF-54-1.0-G38	4.72	−46.2%
SYF-54-1.5-G10	6.01	−36.8%	SYF-54-1.5-G19	5.48	−40.0%	SYF-54-1.5-G38	4.82	−45.1%

### 3.4. Experimental Methods

In order to determine the flowability of all concrete mixtures, the slump test was used by following the ASTM C143/C143M [35] test. Using the slump cylinder, three layers of the concrete mix were inserted evenly. After lifting the cylinder vertically in 5–10 s, the variation between the concrete mixture height and the cylinder height was recorded as the slump value. For the compressive strength test, the average strength of three specimens was measured at 28 days. A compressive testing machine, a control material test system (Control SERCOMP 7 system, CONTROLS S.r.L, Cernusco sul Naviglio, Italy) with a 3000 kN load capacity was used to test the cube specimens. Moreover, the splitting tensile strength tests were conducted at 28 days, utilizing concrete cylinder specimens. For the flexural test, a four-point bending test was conducted on a 150 mm × 150 mm × 550 mm prism. The load was applied using a testing machine with a 300 kN capacity, a control material test system (Control UNIFLEX 300 system, CONTROLS S.r.L, Cernusco sul Naviglio, Italy). The flexural test was performed by following ASTM C78/C78M [33], using a 6 kN/min load rate until the specimen failed.

## 4. Results and Discussions

### 4.1. Effect of Fiber Properties on Flowability

The effects of the fiber type, dosage, and CAMZ on the slump of fresh synthetic/steel FRC are depicted in Figure 3. It should be highlighted that regardless of the fiber type, the fiber inclusion into the concrete damagingly impacted the flowability of fresh FRC. For the micro steel fiber (MSF), maximum slump declines of 7.9%, 23.7%, and 29.8% occurred for MSF concrete with 0.5%, 1.0%, and 1.5% fiber dosages, respectively, compared with the control mix. Additionally, the hooked end steel fiber (HSF) added into the control concrete had higher negative effects on the slump results compared with the MSF mixtures, with the maximum slump decreases being around 10%, 28%, and 34% for HSF concrete with 0.5%, 1.0%, and 1.5% fiber dosages, respectively, for both fiber lengths (35 mm and 60 mm). Moreover, Figure 3c,f shows greater influences from the longest fiber lengths of the HSF and synthetic fiber (SYF) on the flowability compared with the short fibers. The reduction in the fresh concrete flowability with incorporated synthetic/steel fiber might be attributed to the scattering of the fiber in fresh mixture concrete, which established interfacial bonding between the fibers and the concrete matrix [36]. In Figure 3, the results of the slump test reveal that the slump of fresh synthetic/steel fiber mix produced a decreasing tendency

with the synthetic/steel fiber length's increase. Thus, the impact of the fiber–concrete matrix took the lead for the decrease of the mix slump, even though the number of fibers was lower in the same fiber dosage with the same volume of concrete.

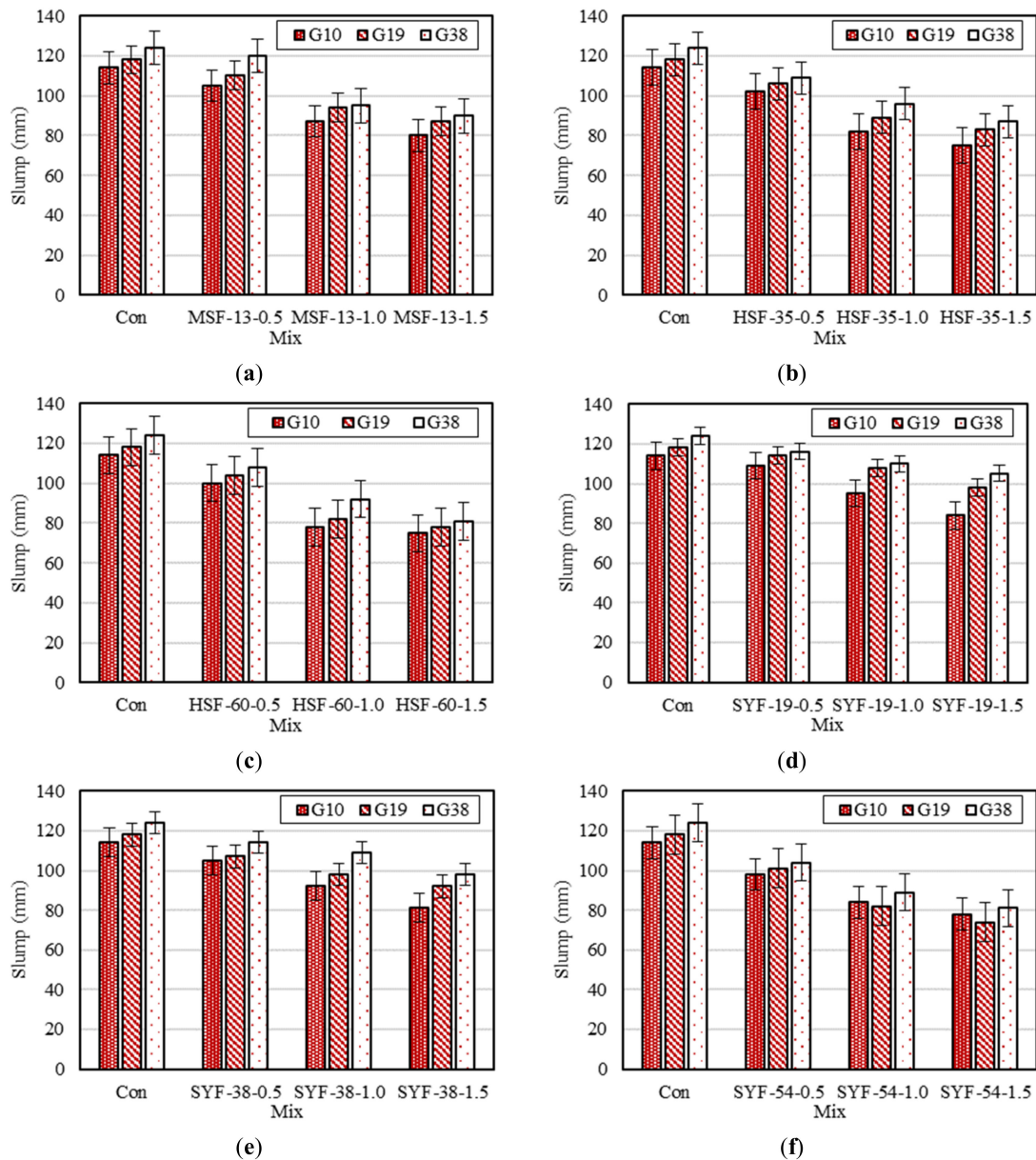


**Figure 3.** Effects of fiber type, dosage, and coarse aggregate maximum size (CAMZ) on the slump for the (a) MSF-13, (b) HSF-35, (c) HSF-60, (d) SYF-19, (e) SYF-38, and (f) SYF-54 fibers.

Furthermore, the slump of fresh synthetic/steel mixture along with control mixture enhanced as the CAMZ increased from 9.5 mm to 37.5 mm [37]. It should be noted that the increase of the CAMZ may decrease the small particle content in the aggregate, which negatively influences the amount of concrete mixture covering the coarse aggregate, causing an increase of the slump [38].

#### 4.2. Effect of Fiber Properties on the Compressive Strength

Figure 4 depicts the compressive strength variations of synthetic/steel FRC versus the fiber type, dosage, and CAMZ. The standard deviation of the compressive strength of the MSF, HSF, and SYF ranged from 2.44 to 2.84 MPa, 2.58 to 3.15 MPa, and 1.89 to 3.14 MPa, respectively, for all CAMZs. Figure 4 shows that the compressive strength of

the control concrete was reduced by increasing the CAMZ, and the percentage decreases were 6.6% and 16.6% for the Con-G19 and Con-G38 mixtures, respectively, compared with the Con-G10 mixture. For specimens with incubating synthetic/steel fiber, the results display that the compressive strength of the FRCs was improved by the incorporation of fibers, and the maximum percentage increases were around 62%, 85%, and 82% for the MSF-13-1.5-G10, MSF-13-1.5-G19, and MSF-13-1.5-G38 mixtures, respectively, compared with the Con mixtures. It should be highlighted that regardless of the fiber type and dosage, the fiber inclusion into the concrete significantly impacted the compressive strength of the FRC. This enhancement may be due to the fact that the fibers can bridge microcracks and macrocracks that form in the concrete matrix [39–42]. It should be highlighted that the compressive strength was only marginally affected by the CAMZ compared with the fiber dosage and geometrical properties, such as the length and diameter, which had an insignificant influence on the compressive strength.

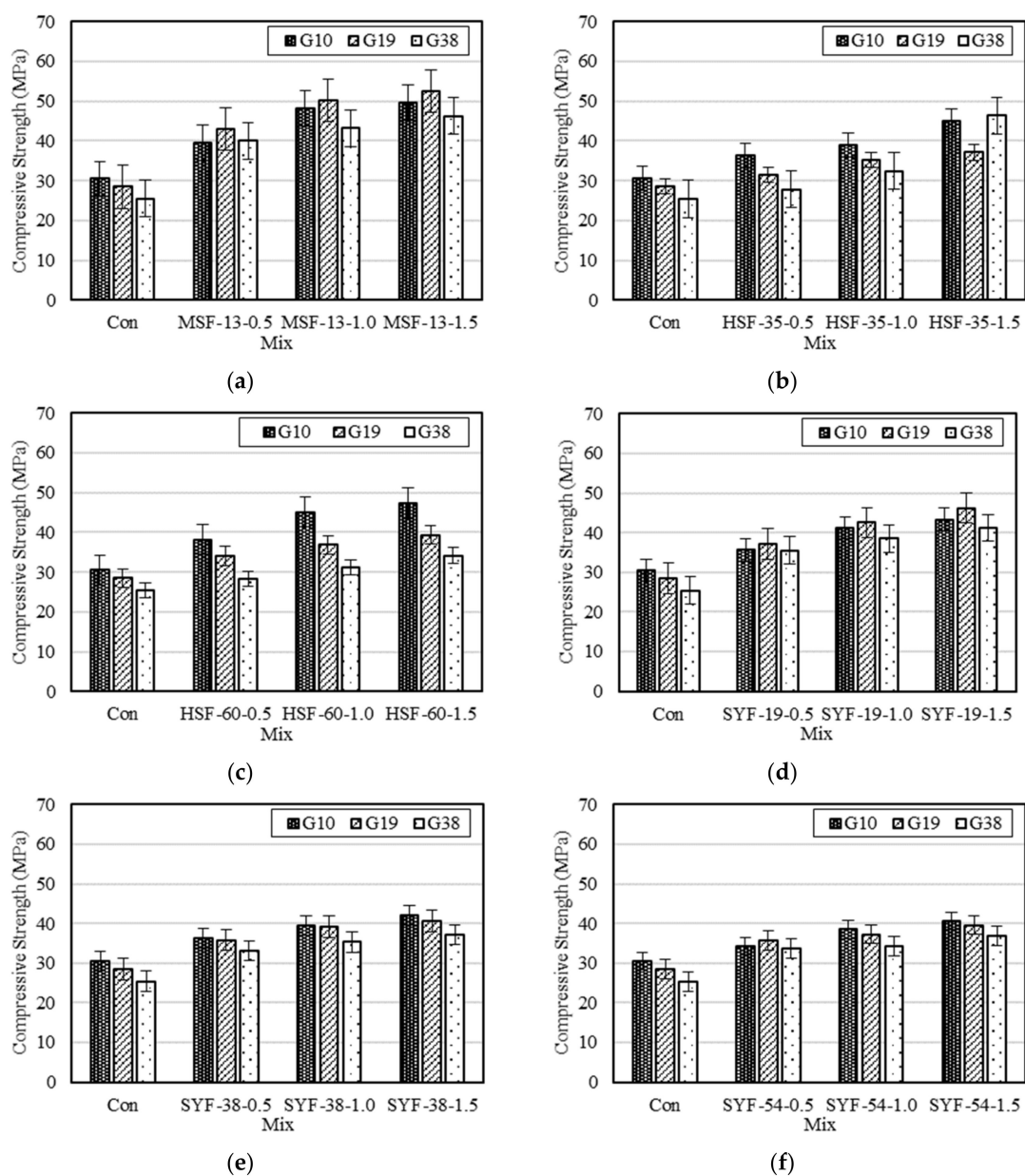


**Figure 4.** Effects of fiber type, dosage, and CAMZ on the compressive strength for the (a) MSF-13, (b) HSF-35, (c) HSF-60, (d) SYF-19, (e) SYF-38, and (f) SYF-54 fibers.

The greatest improvement of the compressive strength was provided by using the MSF with a 1.5% fiber dosage along with a 19 mm CAMZ (G19). This may be due to the fact that the MSF had a higher fiber content among the other fiber types in the same fiber dosage. Therefore, it was expected that the MSF fiber specimens had more bridged fibers compared with the HSF fiber-reinforced specimens. On the other hand, the lowest increase of the compressive strength was provided by using the HSF with a 60 mm length along with a 37.5 mm CAMZ (G38). It should be noted that most HSFs had pulled out from the concrete matrix, while the other fiber types were still engaged by bridging the formed cracks. This performance was primarily credited to each fiber configuration along with their CAMZs.

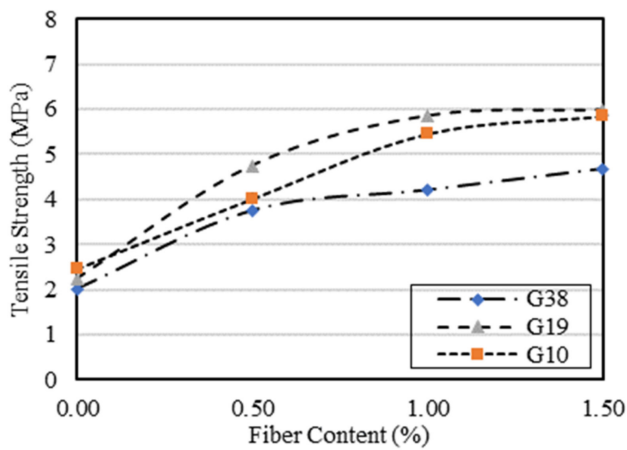
#### 4.3. Effect of Fiber Properties on the Tensile Strength

The effects of the fiber type, dosage, and CAMZ on the splitting tensile strength are presented in Figure 5. The standard deviations of the tensile strengths of the MSF, HSF, and SYF ranged from 0.10 to 0.18 MPa, 0.11 to 0.17 MPa, and 0.12 to 0.26 MPa, respectively, for all CAMZs. From Figure 5, the splitting tensile strength of the control concrete was reduced by increasing the CAMZ, and the percentage decreases were 8.6% and 18.0% for the Con-G19 and Con-G38 mixtures, respectively, compared with the Con-G10 mixture. On the other hand, the results show that adding fiber into the concrete significantly enhanced the tensile strength, with the greatest improvements of 165%, 193%, and 231% occurring for the SYF-54-1.5-G10, SYF-54-1.5-G19, and SYF-54-1.5-G38 mixtures, respectively, compared with the control mixtures. This behavior is primarily recognized as the bond between the concrete matrix and the fiber. Generally, the improvement of the FRC behavior was much more significant in the tension behavior than in the compression behavior.

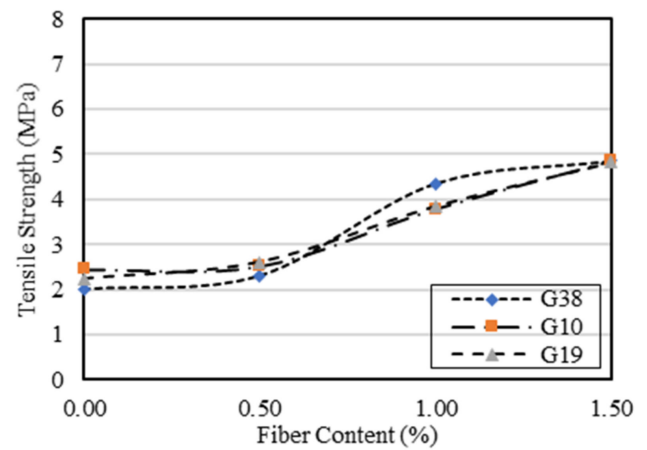
For the specimens with steel fiber, it can be seen that the splitting tensile strength of MSF provided the highest increase compared with the other concrete mixture with hooked end steel fiber types, while the splitting tensile strengths of the synthetic fiber specimens progressively enhanced with the increase of the length of the synthetic fiber. The splitting tensile strength improvement of the synthetic fiber specimens might be due to the synthetic fibers being pulled out after debonding between the fiber and concrete matrix rather than being broken [43]. Thus, a longer embedment length of the synthetic fiber into the concrete matrix can provide larger pullout forces [40–42].

The tensile strengths of the FRC specimens improved with a CAMZ up to 19 mm and then declined with a CAMZ of 37.5 mm, as shown in Figure 5. With the rise of the CAMZ, the total surface area of the coarse aggregate reduced, which decreased the concrete matrix quantity around the aggregate. This may have impacted the fiber-embedded matrix, which led to providing weak pullout forces. Therefore, with the optimum CAMZ, the bonding strength at the interface between the concrete matrix and fiber could be enhanced, and thus the strengthening influence of the fiber on the concrete strength would be enhanced. Nevertheless, the large CAMZ might have a disadvantage in the distribution of fiber in concrete, reducing the strengthening impact of fiber on the concrete strength.

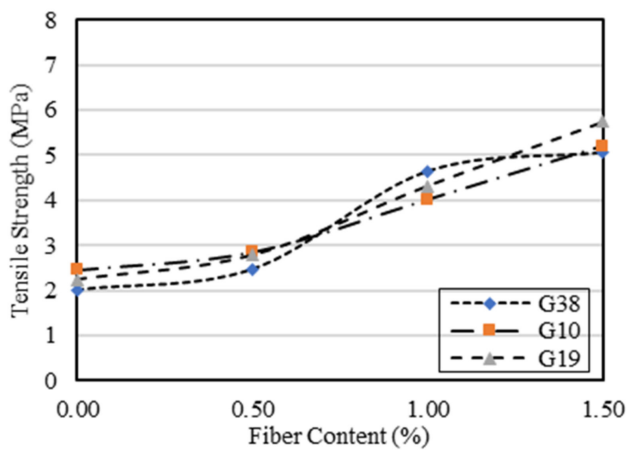
Figure 6 depicts the change rules of the splitting tensile strength ratio of the FRC to the splitting tensile strength of the control concrete with various ratios ( $R_t$ ) of the fiber length to the CAMZ multiplied by the fiber dosage ( $R_t = (l_f/CAMZ) \times f_d$ ). In this figure, the splitting tensile strength ratio significantly rises with the ratio ( $R$ ) increase with good correlation. In addition, there is a significant relationship between the tensile strength ratio and ratio ( $R_t$ ) for all CAMZs. This is primarily accredited to the crack bridging effect formed by the fibers. The bridging effect developed by fibers crossing cracks was improved with the increase of the  $R_t$  factor, which enhanced the FRC mechanical performance. The results demonstrate that the fiber reinforcing effect on the tensile strength was substantial, with the ratio ( $R_t$ ) of the fiber length to the CAMZ multiplied by the fiber dosage ( $R_t = (l_f/CAMZ) \times f_d$ ).



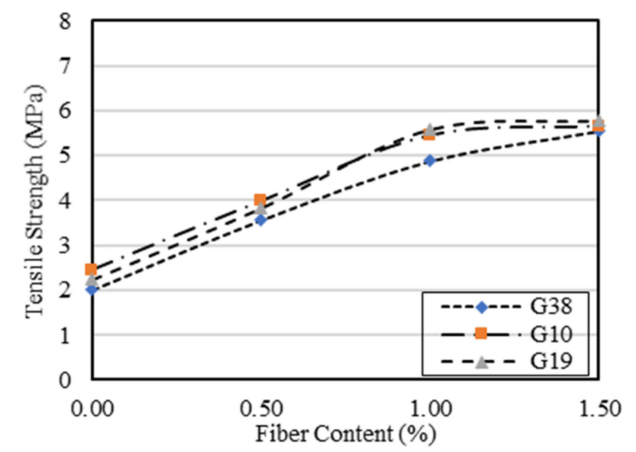
(a)



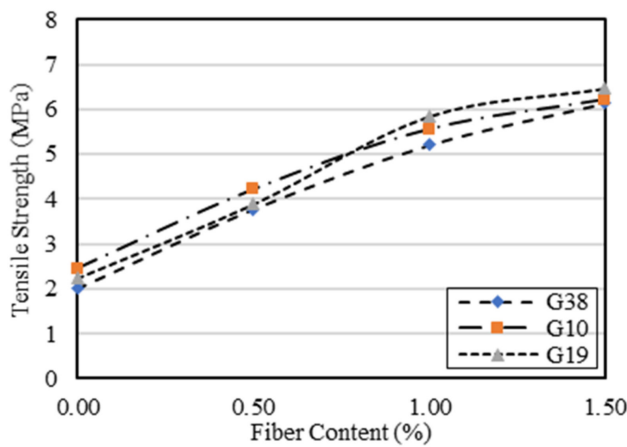
(b)



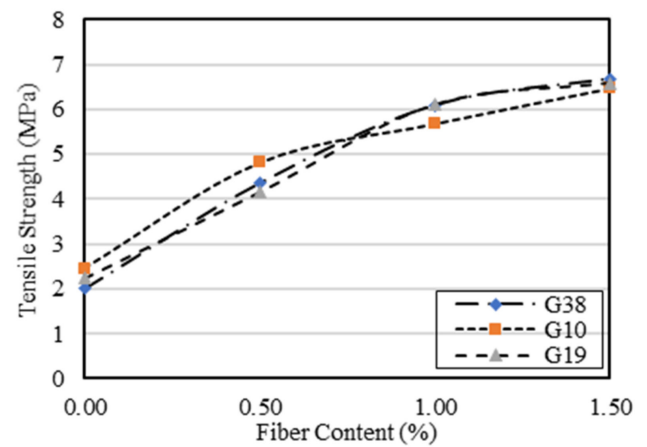
(c)



(d)



(e)



(f)

**Figure 5.** Effects of fiber type, dosage, and CAMZ on the tensile strength for the (a) MSF-13, (b) HSF-35, (c) HSF-60, (d) SYF-19, (e) SYF-38, and (f) SYF-54 fibers.

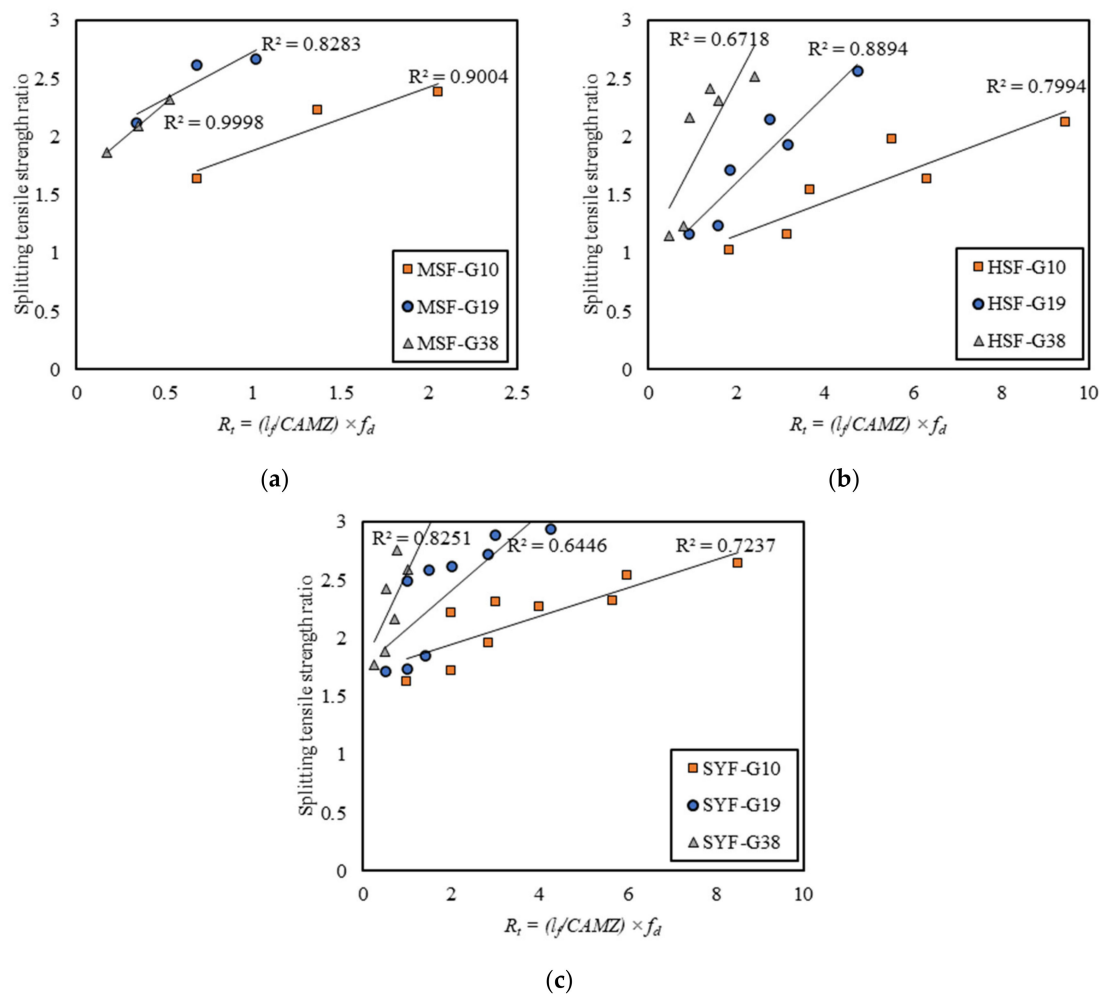


**Figure 6.** Effect of  $R_t = (l_f/CAMZ) \times f_d$  on the tensile strength ratio of (a) micro steel fiber (MSF), (b) hooked end steel fiber (HSF), and (c) SYF specimens.

#### 4.4. Effect of Fiber Properties on the Flexural Strength

Figure 7 demonstrates the effects of the fiber type, dosage, and CAMZ on the flexural strength of synthetic/steel FRCs. The standard deviation of the flexural strength of the MSF, HSF, and SYF ranged from 0.12 to 0.18 MPa, 0.14 to 0.24 MPa, and 0.08 to 0.25 MPa, respectively, for all CAMZs. It should be highlighted the CAMZ decreased the flexural strength by 2.8% and 9.7% for the Con-G19 and Con-G38 mixtures, respectively, compared with the Con-G10 mixture. For the effects of adding synthetic/steel fiber into the control concrete, the flexural strength significantly enhanced, and the maximum increments were 115%, 137%, and 153% for the SYF-38-1.5-G10, SYF-38-1.5-G19, and SYF-38-1.5-G38 specimens, respectively, compared with the Con specimens. This behavior of flexural strength improvement was attributed to the bridging fiber effect, which carried the load after the concrete matrix started cracking until the interfacial debonding between the fibers and the matrix (pulled out) or fiber rupture occurred [16]. In general, the flexural strength of synthetic/steel FRC depicted a trend of improving as the fiber dosage increased. However, the amount of improvement depended on the fiber configuration, as shown in Figure 7. Besides that, the increase of the flexural strength with a CAMZ of 38 mm showed the greatest increase for the synthetic and hooked end steel fiber specimens, while the micro steel fiber specimens exhibited better performance with a CAMZ of 19 mm. Moreover, most of the hooked end fiber had pulled out from the concrete matrix while synthetic fibers were still involved in load transferring across the cracks, as shown in Figure 8. This action was mostly attributed to the configuration of each fiber type. As can be noted, the synthetic

fibers had a larger surface area than the hooked end fibers, causing a higher bond strength between the synthetic fiber and the concrete matrix. Additionally, the same explanations drawn for the differences in tensile strength with the rise of the fiber dosage, length, and CAMZ were primarily accountable for the differences in flexural strength.

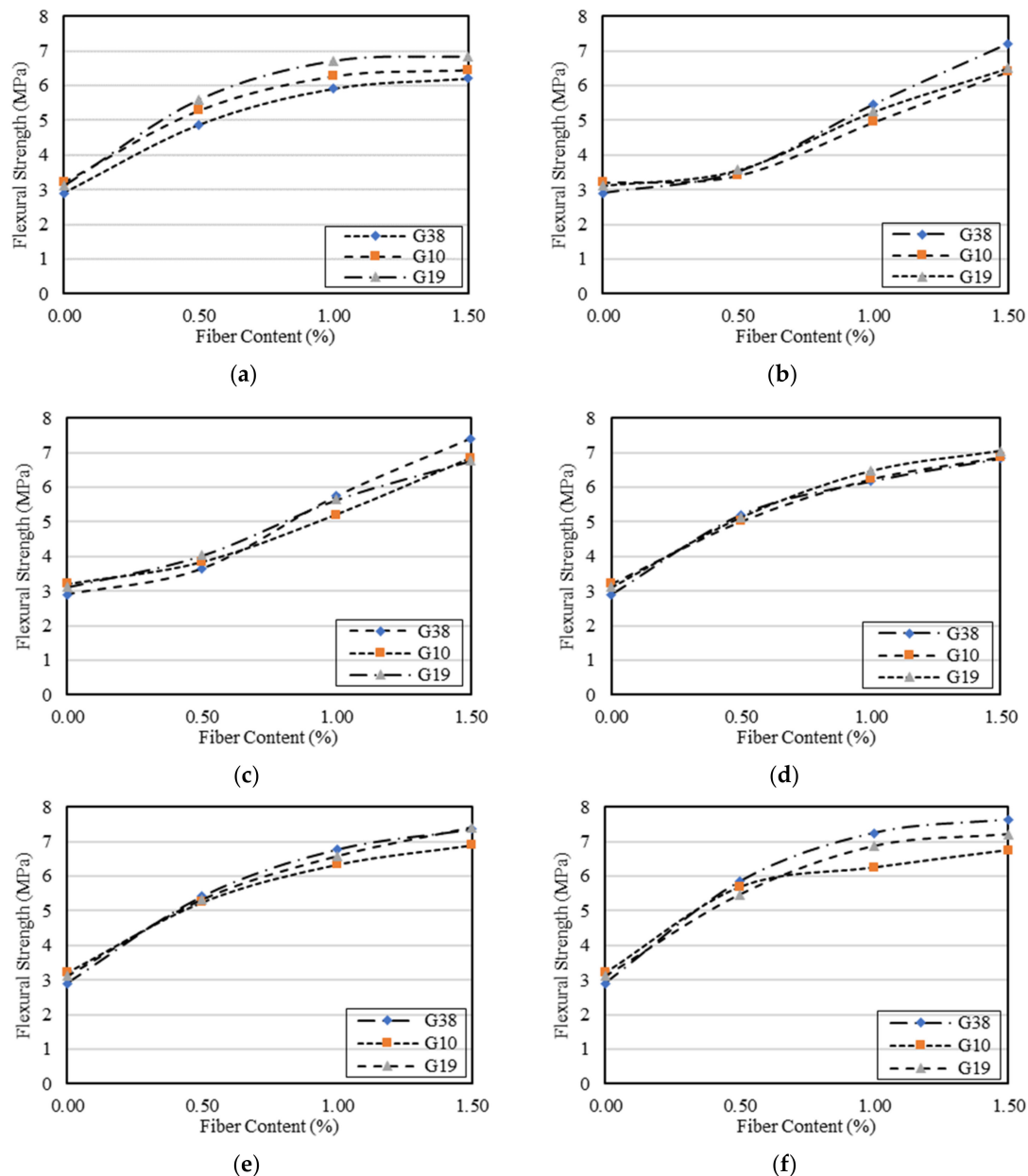


**Figure 7.** Effects of fiber type, dosage, and CAMZ on the flexural strength of (a) MSF-13, (b) HSF-35, (c) HSF-60, (d) SYF-19, (e) SYF-38, and (f) SYF-54 fibers.

Another approach would be to take the effect of the synthetic and steel fiber parameters (fiber length, diameter, and shape) along with the CAMZ on the compressive-to-flexural-strength ratio as the brittleness ratio. The brittleness ratio is the ratio between the compressive strength and the flexural strength listed in Table 8. For the synthetic and steel FRC specimens, the brittleness ratio and percentage changes are presented in Table 8. The low tensile capacity was causing early damage to the concrete, which corresponded to a high brittleness ratio of the concrete. As shown in Table 8, the Con specimens for all CAMZs exhibited the highest brittleness ratios among all synthetic and steel fiber specimens due to the low flexural strength and splitting tensile strength, except for the HSF-35-0.5-G10 and HSF-60-0.5-G10 specimens. This may be due to the inadequate hooked end fiber perfor-

mance with a low fiber dosage and small CAMZ. Moreover, as demonstrated in Table 4, the incorporation of 1.5% synthetic/steel fiber to the concrete mixture significantly reduced the brittleness ratio, increasing the flexural strength compared with the Con specimens. It should be noted that all mixtures were intended to exhibit similar compressive strengths. However, the synthetic/steel fiber advanced the brittleness ratio of specimens with G10, G19, and G38 by approximately 36.8%, 40.7%, and 47.4% greater than the Con specimens, respectively. Additionally, according to Banthia and Sappakittipakorn [39] and Al Rikabi et al. [40–42], due to the fiber's ability to bridge macro and microcracks, the enhancement amount of the flexural strength depended on the fiber dosage and length.

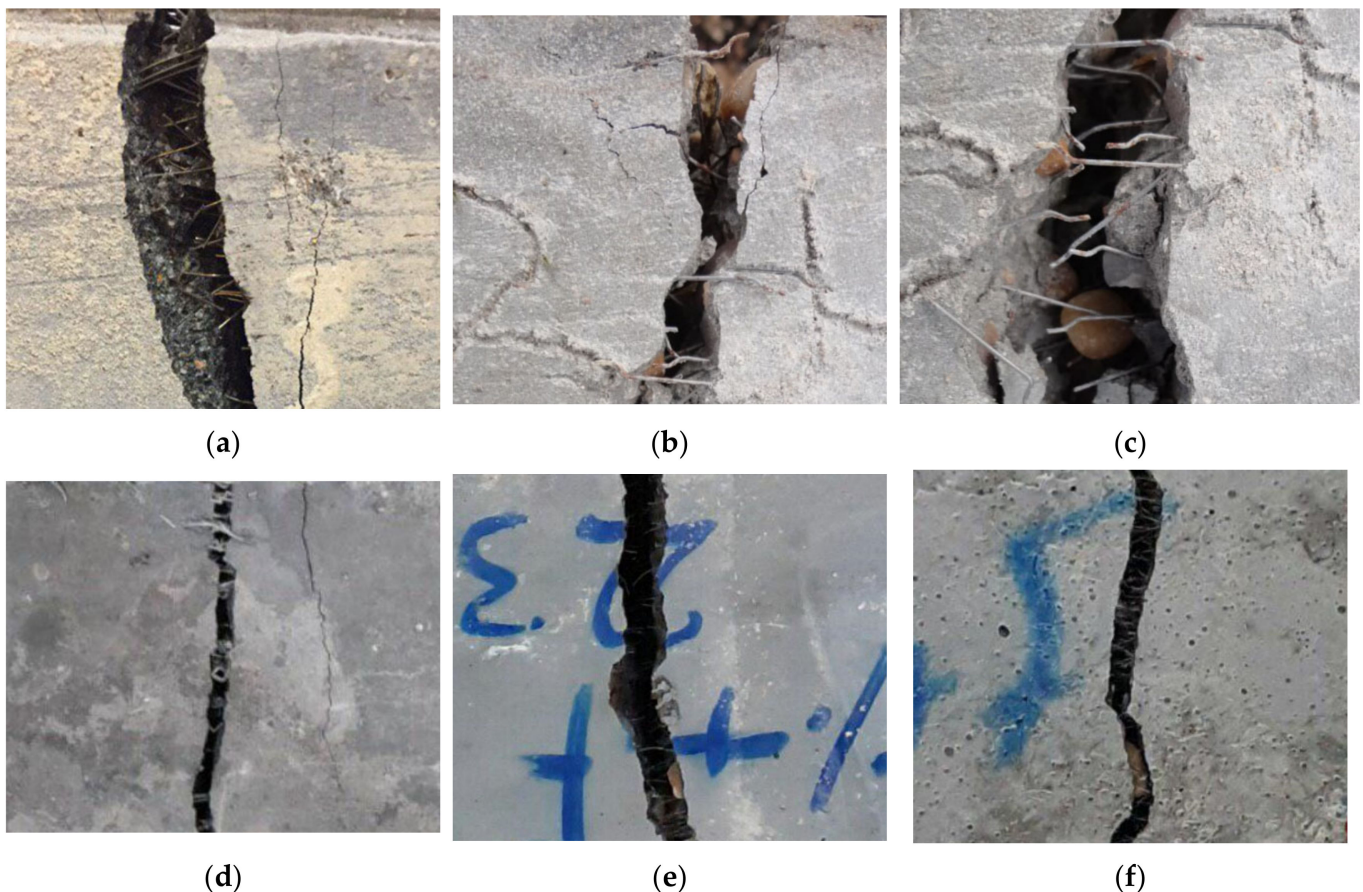


**Figure 8.** Flexural failure mode (a) crack of MSF-13, (b) crack of HSF-35, (c) crack of HSF-60, (d) crack of SYF-19, (e) crack of SYF-38, and (f) crack of SYF-54.

In order to evaluate the impacts of the three main parameters, which are the fiber length ( $l_f$ ), coarse aggregate maximum size (CAMZ), and fiber dosage ( $fd$ ), on the flexural strength of FRC, Figure 9 represents the change rules of the flexural strength ratio of FRC to the flexural strength of the control concrete with various ratios ( $R_f$ ) of the fiber length to the CAMZ multiplied by the fiber dosage ( $R_f = (l_f / \text{CAMZ}) \times fd$ ).

In this figure, the flexural strength ratio significantly rises with the ratio ( $R_f$ ) increase with good correlation. Additionally, there is a significant relationship between the flexural strength ratio and ratio ( $R_f$ ) for all CAMZs. This was mostly attributed to the crack bridging effect formed by fibers. The bridging effect formed by fibers crossing cracks was improved, enhancing the FRC mechanical performance with the increase of the  $R_f$  factor. It is evident that the fiber reinforcing effect on the flexural strength was substantial with the ratio ( $R_f$ ) of the fiber length to the CAMZ multiplied by the fiber dosage ( $R_f$ ).

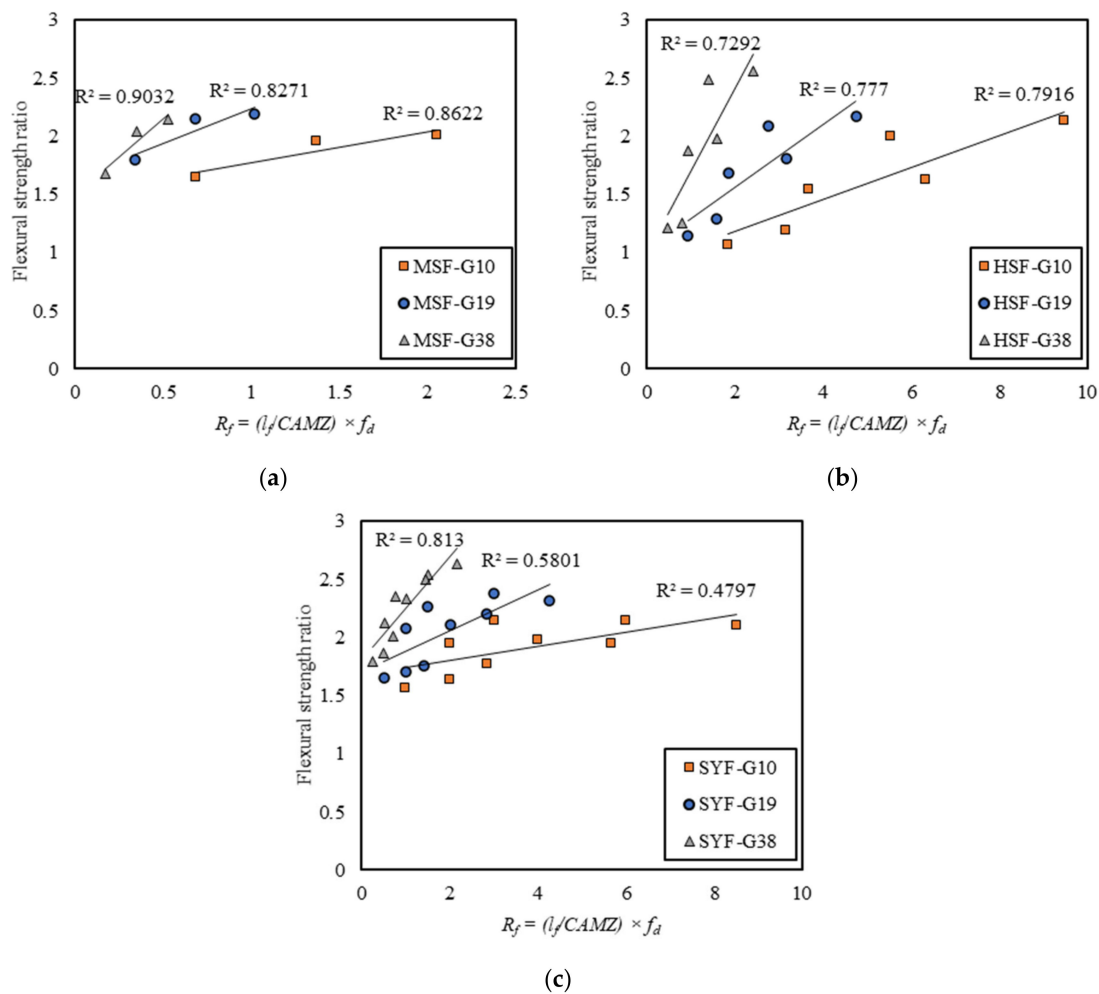


**Figure 9.** Effect of  $R_f = (l_f/CAMZ) \times f_d$  on the splitting tensile strength ratio of (a) micro steel fiber (MSF), (b) hooked end steel fiber (HSF), and (c) SYF specimens.

#### 4.5. Correlations among FRC Properties

To characterize the FRC mechanical properties, past research has used the compressive and tensile strengths as important indicators for essential design requirements in structural design. In order to obtain the concrete tensile strength, the flexural test and splitting tensile test were adopted because they could be operated quickly, easily, and economically compared with the direct tensile test. On the other hand, to estimate the concrete flexural and tensile strengths from the compressive strength, several empirical relations have been recommended by specific design standards and past research [18–29]. Additionally, most of the published empirical relations in use are for plain concrete, while there are limited empirical relations in the literature that could be found for fiber-reinforced concrete [44–46]. Information regarding correlations among the mechanical properties of synthetic and steel FRC with different CAMZs is still limited and unclear. Table 9 shows past research empirical relations between the compressive-tensile strength, flexural-tensile strength, and compressive-flexural strength [44,47–51]. As shown in Table 9, all empirical equations are nonlinearly correlated with the power relation expression, as summarized by Equation (1):

$$f_t = a(f_c')^b \quad (1)$$

where  $f_t$  is the tensile strength or flexural strength,  $f_c'$  is the compressive strength, and  $a$  and  $b$  are coefficients. Therefore, correlations among the FRC compressive strength, splitting tensile strength, and flexural strength were conducted in this section.

**Table 9.** Normal concrete equation from past research.

Compressive Strength and Tensile Strength Relations	
Source	Equation
ACI 318 [47]	$f_t = 0.56(f_{c'})^{0.5}$
CEB-FIP [48]	$f_t = 0.3(f_{c'})^{0.67}$
Choi and Yuan [44]	$f_t = 0.6(f_{c'})^{0.5}$
Xu and Shi [49]	$f_t = 0.21(f_{c'})^{0.83}$
Perumal [50]	$f_t = 0.188(f_{c'})^{0.84}$
Flexural Strength and Tensile Strength Relations	
Source	Equation
Xu and Shi [49]	$f_t = 1.741(f_f)^{0.879}$
Perumal [50]	$f_t = 1.63(f_f)^{0.89}$
Compressive Strength and Flexural Strength Relations	
Source	Equation
ACI 318 [47]	$f_f = 0.62(f_{c'})^{0.5}$
Ahmed and Shah [51]	$f_f = 0.44(f_{c'})^{0.44}$
Xu and Shi [49]	$f_f = 0.39(f_{c'})^{0.39}$
Perumal [50]	$f_f = 0.259(f_{c'})^{0.843}$

#### 4.5.1. Compressive and Splitting Tensile Strengths of FRC

In Figure 10, regression analysis was conducted on the investigational data of the compressive ( $f_{c'}$ ) and splitting tensile strengths ( $f_t$ ) of FRC. From this figure, the empirical relations of different fiber types and configurations found are listed in Table 10. For the MSF-13, SYF-19, SYF-38, and SYF-54 empirical relations, the coefficients of determination ( $R^2$ ) were 0.96, 0.96, 0.91, and 0.86, respectively, indicating a significant correlation. Although the coefficients of determination ( $R^2$ ) of the HSF-35 and HSF-60 were 0.70 and 0.52, respectively, the proposed relations were within an acceptable range [44,52].

Based on the limited empirical relationships between the compressive and tensile strengths of different synthetic and steel fiber parameters and CAMZs, a comparison of the proposed empirical relations from the present study with past research was warranted. In Figure 10, the comparison between the past research predicted curves of the empirical relations and proposed relations along with experimental data points is presented. With the increase of the compressive strength due to the increase of the fiber dosage and decrease of CAMZs, the experimental data points for the control specimens are closer to the CEB FIP [48] curve, as depicted in Figure 10. Additionally, it should be highlighted that the experimental data points with a 0.5% fiber dosage were in good agreement with the ACI 318 [47] and Choe and Yuan [44] curves, while the points with high fiber dosages were close to the proposed curves by Xu and Shi [49] and Nataraja [46]. Therefore, the proposed relationships for different synthetic and steel fiber parameters and CAMZs were established based on experimental data to calculate the tensile strength.

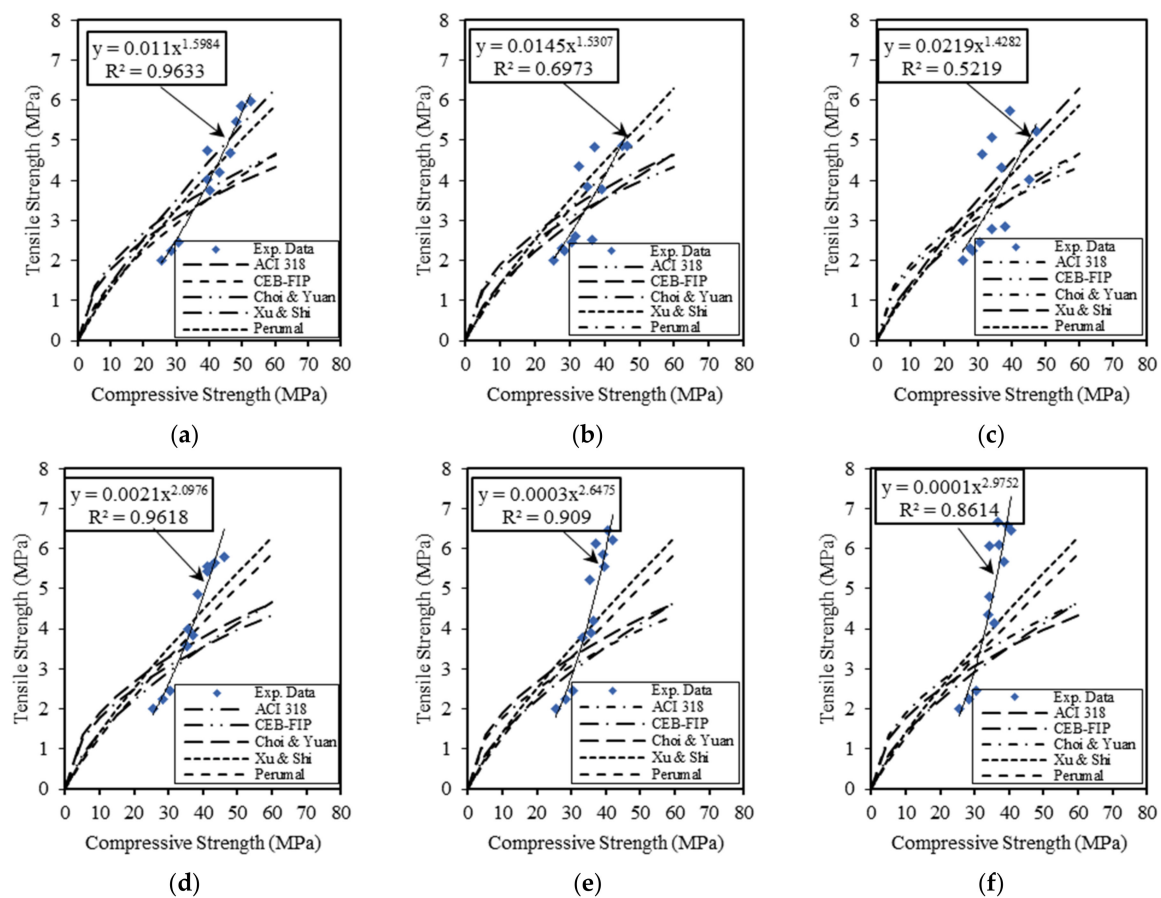


**Figure 10.** Relation between the compressive strength and splitting tensile strength of (a) MSF-13, (b) HSF-35, (c) HSF-60, (d) SYF-19, (e) SYF-38, and (f) SYF-54.

**Table 10.** Summary of compressive strength and tensile strength relations.

Fiber Type	Equation
MSF-13	$f_t = 0.011(f_c')^{1.598}$
HSF-35	$f_t = 0.015(f_c')^{1.531}$
HSF-60	$f_t = 0.022(f_c')^{1.428}$
SYF-19	$f_t = 0.002(f_c')^{2.098}$
SYF-38	$f_t = 0.0003(f_c')^{2.648}$
SYF-54	$f_t = 0.0001(f_c')^{2.975}$

#### 4.5.2. Compressive and Flexural Strengths of FRC

As shown in Figure 11, the compressive ( $f_c'$ ) and flexural strengths ( $f_f$ ) of FRC were produced as experimental data points. In this figure, it can be noted that there was a general trend for all fiber types. Therefore, the regression analysis was conducted, and the empirical relations are listed in Table 11. The coefficients of determination ( $R^2$ ) were 0.96, 0.95, 0.85, and 0.80, respectively, indicating a significant correlation, while the coefficients of determination ( $R^2$ ) of HSF-35 and HSF-60 were 0.70 and 0.49, respectively. For the low  $R^2$  values of HSF fiber relations, the data points may have been impacted by the fiber debonding effect and fiber pullout effect compared with other fiber types, such as MSF and SYF fibers [51].

Past research has proposed empirical relations between the compressive strength and flexural strength, which are listed in Table 9 and depicted in Figure 11. With the increase of the compressive strength due to the increase of the fiber dosage and decrease of CAMZs, the experimental data points for the control specimens were closer to the ACI

318 [47] curve depicted in Figure 11. The investigational data points were noted to be closer to the available empirical relations proposed by Perumal [50] with a high fiber dosage. This observation was accorded with a high correlation for MSF and SYF with different fiber lengths because the synthetic fibers had larger surface areas than the hooked end fibers, causing a higher bond strength between the synthetic fiber and concrete matrix. Additionally, Figure 11 shows a trend of increased flexural strength with an enhancement in the compressive strength due to the increase of the fiber dosage and decrease of CAMZs. Therefore, in this study, the established empirical relations obtained from the experimental data are listed in Table 11.

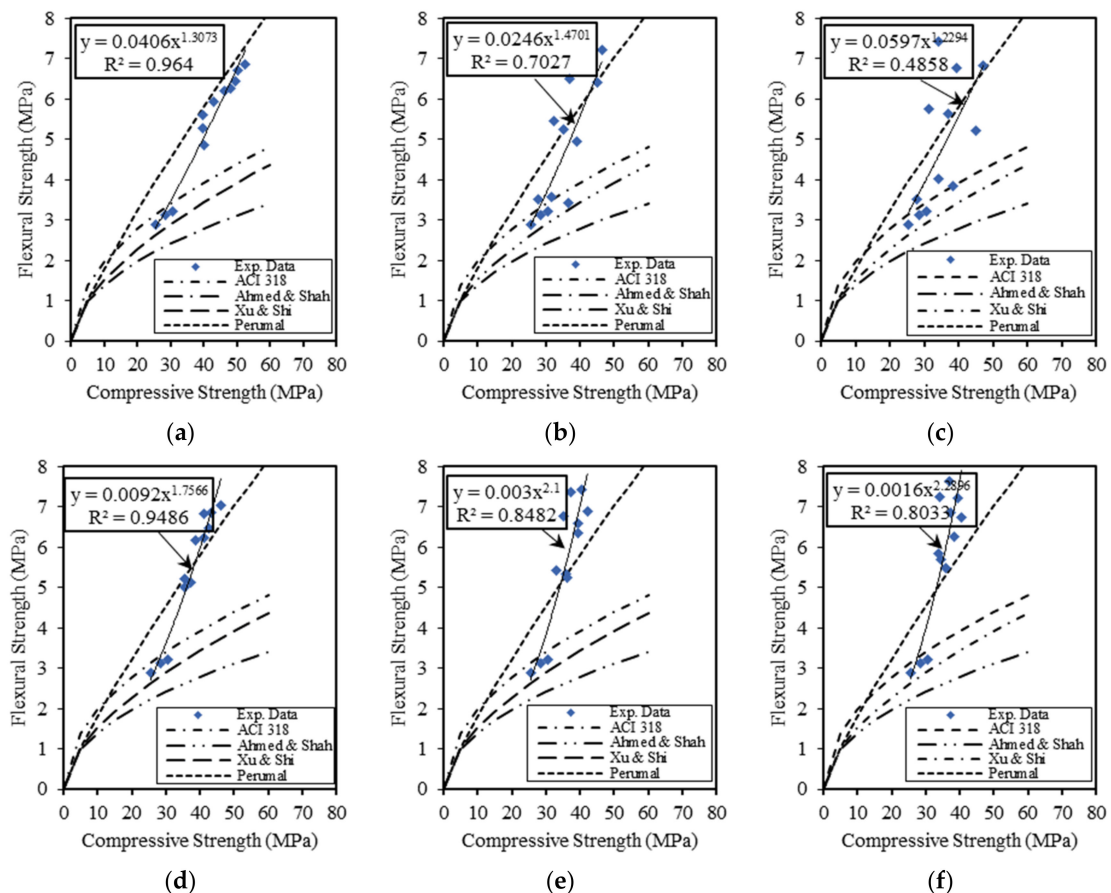


**Figure 11.** Relation between the compressive and flexural strengths of (a) MSF-13, (b) HSF-35, (c) HSF-60, (d) SYF-19, (e) SYF-38, and (f) SYF-54.

**Table 11.** Summary of compressive strength and flexural strength relations.

Fiber Type	Equation
MSF-13	$f_f = 0.041(f_c')^{1.307}$
HSF-35	$f_f = 0.025(f_c')^{1.470}$
HSF-60	$f_f = 0.056(f_c')^{1.229}$
SYF-19	$f_f = 0.009(f_c')^{1.757}$
SYF-38	$f_f = 0.003(f_c')^{2.100}$
SYF-54	$f_f = 0.0016(f_c')^{2.289}$

#### 4.5.3. Splitting Tensile and Flexural Strengths of FRC

The tensile ( $f_t$ ) and flexural strengths ( $f_f$ ) of the FRC correlations are shown in Figure 12 using regression analysis. The empirical relations for all fiber types are listed in Table 12. The coefficients of determination ( $R^2$ ) were 0.97, 0.97, 0.97, 0.98, 0.98, and 0.98 for the

MSF-13, HSF-35, HSF-60, SYF-19, SYF-38, and SYF-54 empirical relations, respectively, indicating a significant correlation. These nonlinear relations showed good agreement compared with the Xu and Shi [49] and Perumal [50] proposed equations, as shown in Figure 12. In addition, in this figure, various empirical relationships between the tensile strength and the flexural strength of concrete with various fiber dosages and decreases of CAMZs are shown. As can be seen, the investigational data points are well below the past research curves by Perumal [50] and Xu and Shi [49]. This may be attributed to the effect of the synthetic and steel fiber parameters (fiber length, diameter, and shape) along with the CAMZ, which may lead to various empirical relations.

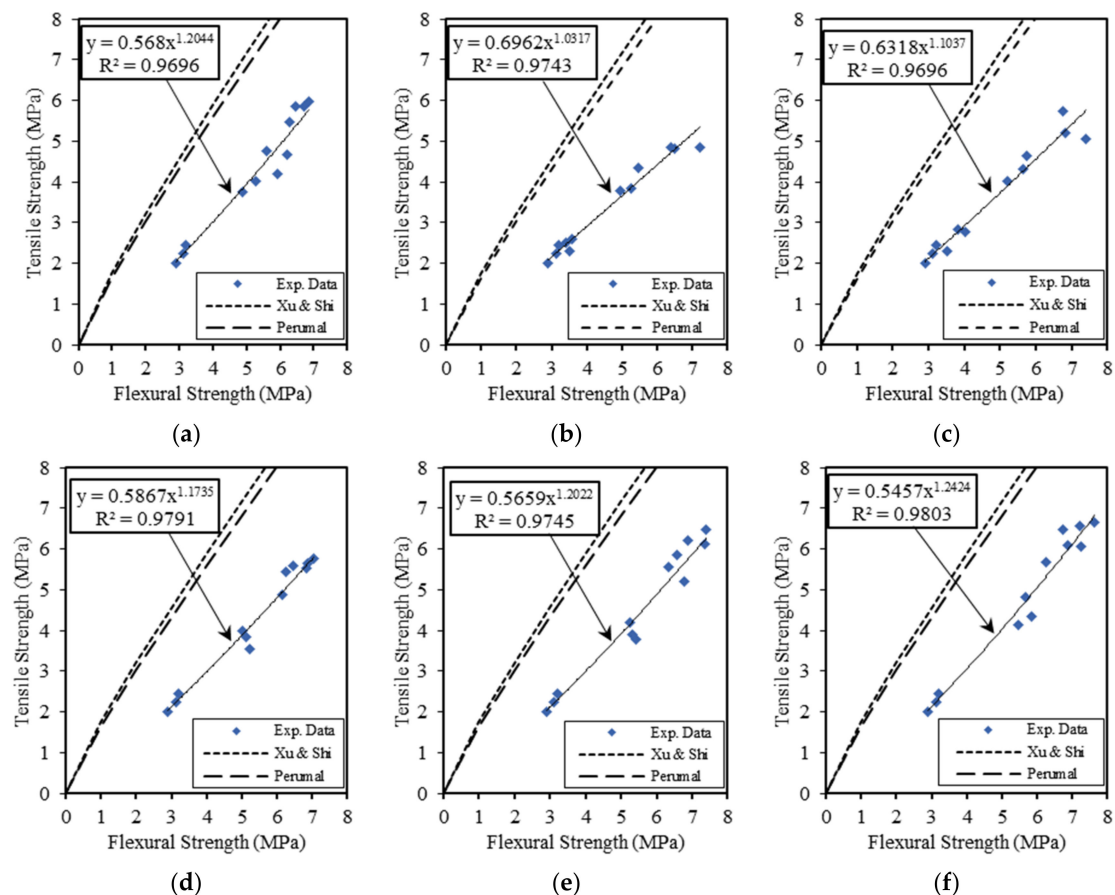


**Figure 12.** Relation between the tensile and flexural strengths of (a) MSF-13, (b) HSF-35, (c) HSF-60, (d) SYF-19, (e) SYF-38, and (f) SYF-54.

**Table 12.** Summary of flexural strength and tensile strength relations.

Fiber Type	Equation
MSF-13	$f_t = 0.568(f_f)^{1.204}$
HSF-35	$f_t = 0.696(f_f)^{1.032}$
HSF-60	$f_t = 0.632(f_f)^{1.104}$
SYF-19	$f_t = 0.587(f_f)^{1.174}$
SYF-38	$f_t = 0.566(f_f)^{1.202}$
SYF-54	$f_t = 0.546(f_f)^{1.242}$

In the present study, the mechanical properties of synthetic and steel FRC could be influenced by many factors, such as the fiber types, steel fiber geometry, fiber parameters,

aspect ratio, and fiber dosage. Additionally, it should be highlighted that the regression analysis investigation was conducted for all compressive strengths, splitting tensile strengths, and flexural strengths of synthetic and steel FRC with the consideration of these factors. These factors were a fiber length ( $l_f$ ) from 13 mm to 60 mm, CAMZ from 9.5 mm to 37.5 mm, and the ratio of  $l_f$ /CAMZ in the range of 0.35–5.68. Therefore, it can be noted that there were strong correlations from the regression analysis of the mechanical property results of the synthetic and steel FRC. It should be highlighted that the fact that all the proposed relations by past research used powers less than one, and that the proposed ones in this study were always bigger than one, was because in this study, the different fiber dosages and CAMZs were used to create the proposed relations. On the other hand, the past research used constant fiber dosages and CAMZs in each study. Therefore, the various ratios ( $R_t$ ) of the fiber length to the CAMZ multiplied by the fiber dosage (see Figure 6) and various ratios ( $R_f$ ) of the fiber length to the CAMZ multiplied by fiber dosage (see Figure 9) were presented. Based on these results, an analysis of the different fiber dosages, fiber lengths, and CAMZs was necessary to fully understand the performance of the correlations among the FRC properties.

## 5. Conclusions

Based on the experimental investigation and regression analysis of the effects of steel and synthetic fiber parameters (fiber length, diameter, shape, and dosage) along with different CAMZs on mechanical properties, the following conclusions were reached:

1. The slump test revealed that the slump of fresh synthetic/steel fiber mix produced a decreasing tendency with the synthetic/steel fiber length's increase. This decline in the fresh concrete flowability might have been due to the fiber length increase, which raised the overlap between fibers. Thus, the impact of the fiber–concrete matrix took the lead for the decrease of the mix slump, even though the number of fibers was lower in the same fiber dosage with the same volume of concrete;
2. The compressive strength was only marginally affected by the CAMZ compared with the fiber dosage and geometrical properties, such as the length and diameter, which had an insignificant influence on the compressive strength;
3. The splitting tensile strength of the FRC specimens improved with a CAMZ up to 19 mm and then declined with a CAMZ of 37.5 mm. With the rise of the CAMZ, the total surface area of the coarse aggregate reduced, which decreased the concrete matrix quantity covering the aggregate. Therefore, the large CAMZ might have had a disadvantage in the fiber distribution of fiber in the concrete that reduced the strengthening impact of the fiber on the concrete strength;
4. There was a significant relationship between the tensile strength ratio and ratio ( $R_t$ ) for all CAMZs. The bridging effect developed by fibers crossing cracks was improved with the increase of the  $R_t$  factor, which enhanced the FRC machinal performance. The results demonstrate that the fiber reinforcing effect on the tensile strength was substantial with the ratio ( $R_t$ ) of the fiber length to the CAMZ multiplied by the fiber dosage ( $R_t = (l_f/\text{CAMZ}) \times fd$ );
5. The synthetic fibers had a larger surface area than the hooked end fibers, causing a higher bond strength between the synthetic fiber and concrete matrix. In addition, the same explanations drawn for the differences in tensile strength with the rise of the fiber dosage, length, and CAMZ were primarily accountable for the differences in flexural strength;
6. All mixtures were intended to exhibit similar compressive strengths. However, the synthetic/steel fiber advanced the brittleness ratios of the specimens with G10, G19, and G38 to be approximately 36.8%, 40.7%, and 47.4% greater than the Con specimens, respectively. Due to the fiber's ability to bridge macro and microcracks, the enhancement amount of flexural strength depended on the fiber dosage and length;
7. The flexural strength ratio significantly rose with the ratio ( $R_f$ ) increase with good correlation. Additionally, there was a significant relationship between the flexural

strength ratio and ratio ( $R_f$ ) for all CAMZs. It is evident that the fiber reinforcing effect on the flexural strength was substantial with the ratio ( $R_t$ ) of the fiber length to the CAMZ multiplied by the fiber dosage ( $R_f$ );

8. The mechanical properties of synthetic and steel FRC could be influenced by many factors, such as the fiber type, steel fiber geometry, fiber parameters, aspect ratio, and fiber dosage. In addition, it should be highlighted that the regression analysis investigation was conducted for all compressive strengths, splitting tensile strengths, and flexural strengths of the synthetic and steel FRC with the consideration of these factors. These factors were a fiber length from 13 mm to 60 mm, CAMZ from 9.5 mm to 37.5 mm, and ratio of the fiber length to the CAMZ in the range of 0.35–5.68. Therefore, it can be noted that there were strong correlations from the regression analysis of the mechanical property results of synthetic and steel FRC.

**Author Contributions:** Data curation, H.M.A.-B.; formal analysis, A.A.I., R.F.H., and H.H.H.; investigation, F.H.A.-M.; methodology, H.M.A.-B. and A.A.I.; project administration, F.H.A.-M.; resources, R.F.H.; supervision, H.H.H.; writing—original draft, R.F.H.; writing—review and editing, H.H.H. All authors have read and agreed to the published version of the manuscript.

**Funding:** This research received no external funding.

**Institutional Review Board Statement:** Not applicable.

**Informed Consent Statement:** Not applicable.

**Data Availability Statement:** The data presented in this study are available on request from the corresponding author.

**Conflicts of Interest:** The authors declare no conflict of interest.

## References

1. Thomas, J.; Ramaswamy, A. Mechanical properties of steel fiber- reinforced concrete. *J. Mater. Civ. Eng.* **2007**, *19*, 385–392. [[CrossRef](#)]
2. Mohammadi, Y.; Singh, S.P.; Kaushik, S.K. Properties of steel fibrous concrete containing mixed fibers in fresh and hardened state. *Constr. Build. Mater.* **2008**, *22*, 956–965. [[CrossRef](#)]
3. Song, P.S.; Hwang, S. Mechanical properties of high-strength steel fiber- reinforced concrete. *Constr. Build. Mater.* **2004**, *18*, 669–673. [[CrossRef](#)]
4. Sahin, Y.; Köksal, F. The influences of matrix and steel fiber tensile strengths on the fracture energy of high-strength concrete. *Constr. Build. Mater.* **2011**, *25*, 1801–1806. [[CrossRef](#)]
5. Grünwald, S.; Walraven, J.C. Parameter-study on the influence of steel fibers and coarse aggregate content on the fresh properties of self- compacting concrete. *Cem. Concr. Res.* **2001**, *31*, 1793–1798. [[CrossRef](#)]
6. Wu, Z.; Shi, C.; He, W.; Wu, L. Effects of steel fiber content and shape on mechanical properties of ultra high performance concrete. *Constr. Build. Mater.* **2016**, *103*, 8–14. [[CrossRef](#)]
7. Ding, X.; Li, C.; Zhao, M.; Li, J.; Geng, H.; Lian, L. Tensile Behavior of Self-Compacting Steel Fiber Reinforced Concrete Evaluated by Different Test Methods. *Crystals* **2021**, *11*, 251. [[CrossRef](#)]
8. Hassan, R.F.; Jaber, M.H.; Al-Salim, N.H.; Hussein, H.H. Experimental research on torsional strength of synthetic/steel fiber-reinforced hollow concrete beam. *Eng. Struct.* **2020**, *220*, 110948. [[CrossRef](#)]
9. Elices, M.; Rocco, C.G. Effect of aggregate size on the fracture and mechanical properties of a simple concrete. *Eng. Fract. Mech.* **2008**, *75*, 3839–3851. [[CrossRef](#)]
10. Appa, G.; Rao, B.K. Raghu Prasad, Fracture energy and softening behavior of high-strength concrete. *Cem. Concr. Res.* **2002**, *32*, 247–252.
11. Khan, M.I.; Abbass, W.; Alrubaidi, M.; Alqahtani, F.K. Optimization of the Fine to Coarse Aggregate Ratio for the Workability and Mechanical Properties of High Strength Steel Fiber Reinforced Concretes. *Materials* **2020**, *13*, 5202. [[CrossRef](#)] [[PubMed](#)]
12. Beygi, M.H.A.; Kazemi, M.T.; Nikbin, M.I.; Amiri, J.V.; Rabbanifar, S.; Rahmani, E. The influence of coarse aggregate size and volume on the fracture behavior and brittleness of self-compacting concret. *Cem. Concr. Res.* **2014**, *66*, 75–90. [[CrossRef](#)]
13. Beygi, M.H.A.; Kazemi, M.T.; Nikbin, M.I.; Amiri, J.V.; Rabbanifar, S.; Rahmani, E. Evaluation of the effect of maximum aggregate size on fracture behavior of self compacting concrete. *Constr. Build. Mater.* **2014**, *55*, 202–211. [[CrossRef](#)]
14. Jang, S.J.; Yun, Y.J.; Yun, H.D. Influence of fiber volume fraction and aggregate size on flexural behavior of high strength steel fiber-reinforced concrete (SFRC). *Appl. Mech. Mater.* **2013**, *372*, 223–226. [[CrossRef](#)]
15. Olivito, R.S.; Zuccarelli, F.A. An experimental study on the tensile strength of steel fiber reinforced concrete. *Composites* **2010**, *41*, 246–255. [[CrossRef](#)]

16. Yao, W.; Cai, J.; Keru, W.; Zhou, Z. Study of flexural toughness of steel fiber reinforced concrete. *Concrete* **2002**, *6*, 30–33.
17. Uygunog̃lu, T. Investigation of microstructure and flexural behavior of steel-fiber reinforced concrete. *Mater. Struct.* **2008**, *41*, 1441–1449. [[CrossRef](#)]
18. Bayramov, F.; Tasdemir, C.; Tasdemir, M.A. Optimisation of steel fiber reinforced concretes by means of statistical response surface method. *Cem. Concr. Compos.* **2004**, *26*, 665–675. [[CrossRef](#)]
19. Yoo, D.-Y.; Kang, S.-T.; Yoon, Y.-S. Effect of fiber length and placement method on flexural behavior, tension-softening curve, and fiber distribution characteristics of UHPFRC. *Constr. Build. Mater.* **2014**, *64*, 67–81. [[CrossRef](#)]
20. Yoo, D.-Y.; Zi, G.; Kang, S.-T.; Yoon, Y.-S. Biaxial flexural behavior of ultra-high-performance fiber-reinforced concrete with different fiber lengths and placement methods. *Cem. Concr. Compos.* **2015**, *63*, 51–66. [[CrossRef](#)]
21. Al-Masoodi, A.H.H.; Kawan, A.; Kasmuri, M.; Hamid, R.; Khan, M.N.N. Static and dynamic properties of concrete with different types and shapes of fibrous reinforcement. *Constr. Build. Mater.* **2016**, *104*, 247–262. [[CrossRef](#)]
22. Blanco, A.; Pujadas, P.; De la Fuente, A.; Cavalaro, S.H.P.; Aguado, A. Assessment of the fiber orientation factor in SFRC slabs. *Compos. Part B* **2015**, *68*, 343–354. [[CrossRef](#)]
23. Sergio, H.; Cavalaro, P.; López, R.; Torrents, J.M.; Aguado, A. Improved assessment of fiber content and orientation with inductive method in SFRC. *Mater. Struct.* **2015**, *48*, 1859–1873.
24. Faris, M.A.; Abdullah, M.M.A.B.; Muniandy, R.; Abu Hashim, M.F.; Bloch, K.; Jež, B.; Ghazali, M.F. Comparison of Hook and Straight Steel Fibers Addition on Malaysian Fly Ash-Based Geopolymer Concrete on the Slump, Density, Water Absorption and Mechanical Properties. *Materials* **2021**, *14*, 1310. [[CrossRef](#)] [[PubMed](#)]
25. Zhang, P.; Yang, Y.; Wang, J.; Hu, S.; Jiao, M.; Ling, Y. Mechanical Properties and Durability of Polypropylene and Steel Fiber-Reinforced Recycled Aggregates Concrete (FRRAC): A Review. *Sustainability* **2020**, *12*, 9509. [[CrossRef](#)]
26. Yardimci, M.Y.; Baradan, B.; Tasdemir, M.A. *Effect of Fine to Coarse Aggregate Ratio on the Rheology and Fracture Energy of Steel Fiber Reinforced Self-Compacting Concretes*; Indian Academy of Sciences: Bengaluru, India, 2014; Volume 39, pp. 1447–1469.
27. Lee, C.; Kim, H. Orientation factor and number of fibers at failure plane in ring- type steel fiber reinforced concrete. *Cem. Concr. Res.* **2010**, *40*, 810–819. [[CrossRef](#)]
28. Kang, S.T.; Lee, B.Y.; Kim, J.K.; Kim, Y.K. The effect of fiber distribution characteristics on the flexural strength of steel fiber-reinforced ultra high strength concrete. *Constr. Build. Mater.* **2011**, *25*, 2450–2457. [[CrossRef](#)]
29. ASTM. C150-04a. *Standard Specification for Portland Cement*; ASTM International: West Conshohocken, PA, USA, 2004.
30. ASTM. C33-03. *Standard Specification for Concrete Aggregates*; ASTM International: West Conshohocken, PA, USA, 2003.
31. BSI. BS EN 12390-3. *Testing Hardened Concrete. Compressive Strength of Test Specimen*; BSI: London, UK, 2009.
32. ASTM. C496/C496M-17. *Standard Test Method for Splitting Tensile Strength of Cylindrical Concrete Specimens*; ASTM International: West Conshohocken, PA, USA, 2017.
33. ASTM. C78/C78M-10. *Standard Test Method for Flexural Strength of Concrete (Using Simple Beam with Third-Point Loading)*; ASTM International: West Conshohocken, PA, USA, 2010.
34. ASTM. C31/C31M-12. *Standard Practice for Making and Curing Concrete Test Specimens in the Field*; ASTM International: West Conshohocken, PA, USA, 2012.
35. ASTM. C143/C143M-20. *Standard Test Method for Slump of Hydraulic-Cement Concrete*; ASTM International: West Conshohocken, PA, USA, 2020.
36. Yap, S.P.; Khaw, K.R.; Alengaram, U.J.; Jumaat, M.Z. Effect of fiber aspect ratio on the torsional behavior of steel fiber-reinforced normal weight concrete and lightweight concrete. *Eng. Struct.* **2015**, *101*, 24–33. [[CrossRef](#)]
37. Han, J.; Zhao, M.; Chen, J.; Lan, X. Effects of steel fiber length and coarse aggregate maximum size on mechanical properties of steel fiber reinforced concrete. *Constr. Build. Mater.* **2019**, *209*, 577–591. [[CrossRef](#)]
38. Zhao, S.; Qian, X.; Chen, J.; He, R. Experimental study on the effect of coarse aggregate on the performance of steel fiber reinforced concrete. *China Concr. Cem. Prod.* **2006**, *5*, 45–48.
39. Banthia, N.; Sappakittipakorn, M. Toughness enhancement in steel fiber reinforced concrete through fiber hybridization. *Cem. Concr. Res.* **2007**, *37*, 1366–1372. [[CrossRef](#)]
40. Al Rikabi, F.T.; Sargand, S.M.; Khoury, I.; Hussein, H.H. Material properties of synthetic fiber-reinforced concrete under freeze-thaw conditions. *J. Mater. Civ. Eng.* **2018**, *30*, 04018090. [[CrossRef](#)]
41. Al Rikabi, F.T.; Hussein, H.H.; Khoury, I. Experimental study on shear strength of synthetic fiber reinforced high strength concrete containing slag aggregate. In *Structures Congress 2019: Buildings and Natural Disasters*; American Society of Civil Engineers: Reston, VA, USA, 2019; pp. 179–187.
42. Al Rikabi, F.T.; Sargand, S.M.; Kurdziel, J.; Hussein, H.H. Experimental investigation of thin-wall synthetic fiber-reinforced concrete pipes. *ACI Struct. J.* **2018**, *115*, 1671–1681. [[CrossRef](#)]
43. Choi, O.C.; Lee, C. Flexural performance of ring-type steel fiber-reinforced concrete. *Cem. Concr. Res.* **2003**, *33*, 841–849. [[CrossRef](#)]
44. Choi, Y.; Yuan, R.L. Experimental relationship between splitting tensile strength and compressive strength of GFRC and PFRC. *Cem. Concr. Res.* **2006**, *35*, 1587–1591. [[CrossRef](#)]
45. Ramadoss, P.; Nagamani, K. Investigation on the tensile strength of high- performance fiber reinforced concrete using statistical methods. *Comput. Concr.* **2006**, *3*, 389–400. [[CrossRef](#)]
46. Nataraja, M.C.; Dhang, N.; Gupta, A.P. Splitting tensile strength of SFRC. *Indian Concr. J.* **2001**, *75*, 287–290.

47. ACI Committee 318. *Building Code Requirements for Structural Concrete and Commentary*; American Concrete Institute: Farmington Hills, MI, USA, 1999.
48. CEB-FIP Model Code for Concrete Structures. *Evaluation of the Time Dependent Behavior of Concrete. Bulletin Information No. 199*; Comite Europe du Beton/Federation Internationale de Precontrainte: Lausanne, Switzerland, 1991.
49. Xu, B.W.; Shi, H.S. Correlations among mechanical properties of steel fiber reinforced concrete. *Con. Build. Mat.* **2009**, *23*, 3468–3474. [[CrossRef](#)]
50. Perumal, R. Correlation of compressive strength and other engineering properties of high-performance steel fiber-reinforced concrete. *J. Mater. Civ. Eng.* **2015**, *27*, 1–8. [[CrossRef](#)]
51. Ahmad, S.H.; Shah, S.P. Structural properties of high strength concrete and its applications for precast prestressed concrete. *PCI J.* **1985**, *30*, 97–123.
52. Wang, Z.L.; Wu, J.; Wang, J.G. Experimental and numerical analysis on effect of fibre aspect ratio on mechanical properties of SRFC. *Constr. Build. Mater.* **2010**, *24*, 559–565. [[CrossRef](#)]